Letter

Identification of Surface Sites for Low-Temperature Heterogeneously Catalyzed CO Oxidation on Rh(111)

Rachael Gabrielle Farber, Marie E Turano, and Daniel R Killelea

ACS Catal., **Just Accepted Manuscript** • DOI: 10.1021/acscatal.8b03887 • Publication Date (Web): 01 Nov 2018

Identification of Surface Sites for Low-Temperature Heterogeneously Catalyzed CO Oxidation on Rh(111)

Rachael G. Farber[†] *, Marie E. Turano, and Daniel R. Killelea**

Department of Chemistry & Biochemistry, Loyola University Chicago, 1068 W. Sheridan Rd., Chicago, IL 60660.

[†]*Present Address:* The James Franck Institute and Department of Chemistry, The University of Chicago, 929 East 57th Street, Chicago, Illinois 60637, USA

Abstract

In heterogeneously catalyzed oxidation reactions on metal surfaces, advantageous oxygenaceous species proffer lower barrier reaction pathways. In order to utilize such reactions better, it is essential to understand what species are present, how they are formed, and under what conditions they are available for reaction. Oxides, adsorbed oxygen, and subsurface oxygen each form on Rh(111) surfaces and thus provide the opportunity to distinguish the contributions of each species to overall reactivity. In an effort to elucidate relevant reaction mechanisms on catalytically active rhodium surfaces, a combination of scanning tunneling microscopy (STM) and temperature programmed desorption (TPD) showed that when subsurface oxygen is present, CO was readily oxidized at the interface between the metallic and oxidic phases at relatively modest temperatures.

Keywords Ultra-high vacuum; Heterogeneous catalysis; Scanning Tunneling Microscopy; Rh oxide; CO oxidation

Introduction

The activity of catalytic surfaces is determined by the chemical species present. To further understand and utilize the complex surface chemistry of solid catalysts, it is crucial to obtain atomistic mechanisms for heterogeneously catalyzed reactions. On metals, different chemical species on inhomogeneous surfaces may arrange themselves in spatially separate phases, each with their own characteristic structure. Surface analysis that distinguishes among these structures and follows their evolution with reaction progress provides the means to connect a specific surface species to a particular reaction. Such a level of detail is achievable using robust surface science studies of single crystal transition metals under ultra-high vacuum (UHV) conditions. Such methods provide highly detailed surface characterization as well as fine control of reagent exposures. Therefore, they are uniquely poised to provide the detailed information necessary to further our understanding of the fundamental chemistry of catalytically active surfaces.

It is first necessary to devise approaches where the surface species found under actual catalytic conditions can be prepared in UHV-compatible fashions, whereupon they can be carefully studied and characterized in manners not feasible under high temperature and pressure conditions. Despite the difference in chemical potentials at the two pressure extremes, such studies are important for understanding the fundamental reactivity of catalytically relevant surfaces. Approaches such as atomic oxygen (AO) plasmas[1-2] and gas phase AO exposures[3-5] reproduce the oxide surface structures found after high pressure and temperature O_2 preparations.[6] Such preparation methods established strategies that effectively bridge the "pressure gap".[7-10] A significant result for Rh catalyzed reactions has been the discovery that oxide surfaces, in addition to metallic surfaces, are catalytically active and may surpass the

metallic surface in reactivity.[11-14] There is, however, still debate on the active phase under reaction conditions.[15-18] In particular, it is unclear how an excess of oxygen, in the form of subsurface oxygen (O_{sub}), alters the reaction mechanism and surface oxygen repopulation.

An increase in the amount of oxygen on a metal surface may lower the activation energy (E_a) for catalytic oxidation.[19] As we will describe, exposure of Rh(111) to AO resulted in the incorporation of the equivalent of 3.74 monolayers (ML, 1 ML = 1.6×10^{15} O cm^{-2})[3] of oxygen and promoted CO oxidation at reduced temperatures compared to the 0.5 ML (2×1)-O adlayer. However, the exact reaction mechanism at reduced temperatures is unknown. Besides reduction of E_a at elevated O coverages, there were potential geometric effects that may have altered the reactivity of an oxidic surface. For example, when the proper facet of an oxide was accessible to reactants, otherwise unlikely reactions proceed rapidly.[2, 20] Recently, Liang *et al*.[21] demonstrated low temperature methane activation on rutile IrO_2(110) grown on an Ir(100) single crystal. There, the IrO_2(110) surface exposed coordinatively unsaturated (cus) Ir-O surface pairs that were essential for the observed methane reactivity at low temperatures. Such findings support the role of high oxygen concentrations in lowering energetic barriers and providing advantageous surface and electronic geometries that enable low temperature reactivity on oxygen rich surfaces, such as the Rh(111) crystal in this work.

In this work, the oxidation of CO over highly oxidized Rh(111) surfaces was studied to elucidate the active sites for CO oxidation. A combination of temperature programmed desorption (TPD) and scanning tunneling microscopy (STM) were used to quantify the oxygen coverage (θ_O) on and in the Rh(111) sample and determine surface structure. The oxygenaceous species and their abundances were controlled by the duration of exposure to gas-phase AO and

selection of the Rh(111) temperature during AO exposure ($T_{S,AO}$). Depending on the exposure conditions, the surface composition could be varied from being uniformly covered in a (2×1)-O adlayer structure with an θ_O = 0.5 ML,[3] or was an inhomogeneous mixture of metallic (2×1)-O and surface oxide (RhO_2) domains with dissolved oxygen atoms in the selvedge of the metal (O_{sub}), demonstrated in previous work.[3] The prepared surface was then exposed to CO at either 300 K or 200 K ($T_{s,CO}$). STM images showed the evolution of the Rh(111) surface following CO exposure and subsequent CO oxidation. Degeneration of particular surface domains indicated *which* domains were more active towards oxidation. The *total* reactivity was determined using TPD to track the oxygen coverage remaining ($\theta_{O,res}$) on the surface after CO oxidation. In this manner, we have revealed that it is the boundary between the metallic and oxidic surface phases that provided lower barrier reaction pathways for oxidation as well as depletion of O_{sub}.

Experimental

Experiments were performed in a UHV apparatus comprised of a preparation chamber and a scanning tunneling microscope (UHV-STM, RHK Technology, Troy, MI) chamber described previously.[5] The Pan-style STM was cooled using a closed-cycle He cryostat, enabling imaging at 30 K. The Rh(111) crystal (Surface Preparation Laboratory, Zaandam, NL) was mounted on a Ta sample holder with a type-K thermocouple. The Rh(111) sample was cleaned with repeated cycles of Ar^+ sputtering and annealing at 1300 K. Surface cleanliness was verified with Auger electron spectroscopy (AES), a clean (1×1) low energy electron diffraction (LEED) pattern, and STM imaging of the atomic lattice. AO was generated using a hot Ir filament as previously reported.[5, 22-23] TPD spectra were recorded with a UTI 100c quadrupole mass spectrometer controlled by a homebuilt labVIEW program. Rh(111) exposed to O_2 at T_s = 350 K resulted in the saturated (2×1)-O 0.5 ML O_{ad} surface; the integral of the O_2 TPD spectra

was used to calibrate subsequent oxygen coverages. AO exposure at $T_{s,AO}$ = 700 K resulted in the RhO_2/(2×1)-O surface.[1] TPD spectra from 100-600 K used a ramp rate of 4 K s^{-1}, and tracked desorption of CO and formation of CO_2 during the temperature ramp. TPD spectra from 400-1400 K used a ramp rate of 3 K s^{-1}, and tracked $\theta_{O,res}$. No CO or CO_2 desorption from the Rh(111) surface were observed in this higher temperature ramp. All STM images were taken at 30 K. TPDs taken after STM imaging were indistinguishable from those where no imaging was performed, indicating that neither background gases accumulated nor did the surface degrade during prolonged STM experiments.[24]

Results and Discussion

The oxidation of CO by adsorbed O atoms (O_{ad}) on Rh(111) is a prototypical reaction for surface-catalyzed oxidation, and therefore has attracted much attention over the years.[25-28] It is known that O_2 dissociates on Rh(111) until θ_O saturates at 0.5 ML O, resulting in a (2×1)-O adlayer. [5, 29] Exposure of a (2×1)-O covered Rh(111) surface to gas-phase CO molecules at 300 K yielded a (2×2)-O+CO overlayer[29-30] from CO insertion into the (2×1) adlayer; this structure has been found to retain θ_O = 0.5 ML, with the addition of 0.25 ML CO. Representative TPD spectra of CO_2 and O_2 desorption from the (2×2)-O+CO, prepared by exposing the (2×1)-O Rh(111) to 60 L CO at 300 K, are provided in Figure S1. The CO_2 desorption spectrum shows that CO oxidation did not occur until the surface temperature was above 350 K and $\theta_{O,res} \approx 0.25$ ML remained on the surface. As previously reported, quantification of the amount of CO oxidized is not necessarily straightforward,[30] and because of experimental restrictions we were unable to directly quantify CO_2 from the TPD spectra. However, because the background for m/z = 32 (O_2^+) was much lower, we were able to quantify the amount of *oxygen* consumed in the oxidation reaction using $\theta_{O,res}$, which provided an indicator for the extent of CO oxidation.

There did not appear to be any differences in the TPD spectra if the CO exposure was done at either $T_{S,CO}$ = 100 K or 300 K, both the apparent CO_2 yield and $\theta_{O,res}$ were not appreciably different, indicating that the O+CO overlayer was stable at 300 K on the experimental timescale.[31] These results showed that in the absence of O_{sub} or the RhO_2 surface oxide, only adsorbed CO was oxidized, and the reaction was limited by the amount of CO adsorbed to the (2×1)-O surface. As we will show, this was not the case when O_{sub} and RhO_2 oxide are present.

In a previous publication, we demonstrated that AO readily oxidizes Rh(111), and large amounts (> 5 ML) of O_{sub} were generated beneath comparatively low θ_O (< 0.75 ML) surfaces.[3] When Rh(111) was oxidized at $T_{s,AO}$ = 700 K, brims of RhO_2 formed at the top of step edges, as indicated by a hexagonal moiré pattern of the (8×8) oxide trilayer on top of a (9×9) Rh substrate[3, 32] in the STM images and LEED patterns. These oxide domains grew with increasing exposure, but covered, at most, half of the surface after a 600 s exposure. Interestingly, the (2×1)-O adlayer covered the rest of the surface, despite the presence of the equivalent of more than 8 ML of oxygen in total ($\theta_{O,total}$) as indicated by the TPD spectra. For $\theta_{O,total}$ above 0.5 ML, there was a sharp desorption peak around 800 K in the TPD spectra that grew roughly linearly with AO exposure.[3] Yet the surface coverage of the oxidized (2×1)-O/RhO_2 Rh(111) surface never exceeded $\theta_O \approx 0.66$ ML, as measured using AES, and this coverage correlates well with the mixture of oxide and (2×1)-O. Because the oxygen surface coverage does not account for $\theta_{O,total}$, the excess O must be present as O_{sub}. O_{sub} are dissolved oxygen atoms in the selvedge of the metal that occupy interstitial spaces, as opposed to the oxygen incorporated into the lattice of the RhO_2 trilayer that happen to reside beneath the layer of Rh atoms. O_{sub} has been previously identified by the telltale sharp desorption peak at 800 K preceding the broad O_{ad} desorption feature from 800 to 1300 K in TPD spectra.[3, 5, 33-34]

We wished to study how the presence of O_{sub} and the RhO_2 oxide affect CO oxidation compared to O_{ad} in the co-adsorbed (2×2)-O+CO structure. To do this, we prepared Rh(111) with high oxygen incorporation, exposed it to CO at $T_{s,CO}$ = 300 K, where little to no reaction was expected to occur, and then used $\theta_{O,res}$ to quantify CO oxidation. Additionally, STM images obtained after CO exposure were analyzed to determine which portions of the surface were most effected by the oxidation reaction. This information would determine which oxygenaceous phases were relatively more reactive; less reactive phases remain on the surface after desorbing CO and CO_2. AO oxidized the Rh(111) at $T_{s,AO}$ = 700 K, giving $\theta_{O,total}$ = 3.74 ML, as shown by the black trace in Figure 1. However, as shown in Figure 1, simply exposing this surface to CO at $T_{s,CO}$ = 300 K resulted in extensive CO oxidation that rapidly consumed not only the surface O, but O_{sub} as well.

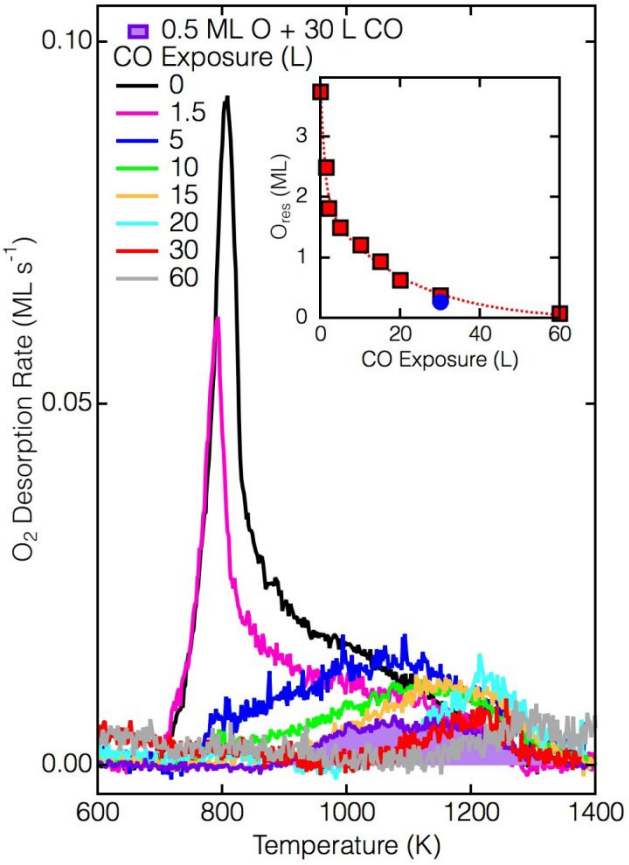

Figure 1. O_{res} (ML) TPD spectra for a $\theta_{O,total}$ = 3.74 ML Rh(111) surface exposed to various exposures of CO (L) at $T_{s,CO}$ = 300 K. Inset - integrated TPD values for O_{res}. Blue circle corresponds to O_{res} from 0.5 ML O + 30 L CO.

Figure 1 shows O_2 desorption TPDs taken after various exposures of the heterogeneous RhO_2, (2×1)-O, and O_{sub} Rh(111) crystal with $\theta_{O,total}$ = 3.74 ML. The TPDs clearly show that the amount of oxygen remaining on the Rh(111) surface dropped precipitously with CO exposure. Even after a modest

CO exposure of 1.5 ML (which would not even saturate the (2×1)-O adlayer), only half of the initially deposited 3.74 ML of oxygen remained ($\theta_{O,res}$ = 1.8 ML) . This was in sharp contrast to (2×2)-O+CO, where, following a 30 L CO exposure, 0.25 ML adsorbed CO reduced the initially deposited 0.5 ML O to 0.25 ML O during the TPD ramp. For longer CO exposures, $\theta_{O,res}$ decreased, roughly exponentially, until it was difficult to detect O_2 desorption above the m/z = 32 background of the chamber. The dramatic decrease in $\theta_{O,res}$ from 3.74 ML to below detection limits showed that the heterogeneous Rh(111) surface was significantly more reactive than the (2×1)-O adlayer. Even though O_{sub} was stably absorbed up to 700 K (as shown in TPD experiments), it was rapidly consumed during CO exposures significantly lower than its desorption temperature, which should be correlated to O_{sub} having sufficient thermal energy to emerge to the surface. The fact that O_{sub} was removed suggests that it was mobile at 300 K and emergent O atoms were highly reactive.

Comparison of the apparent CO_2 yields from the $\theta_{O,total}$ = 3.74 ML to the $\theta_{O,total}$ = 0.5 ML (2×1)-O surface (Table S1) showed the amount of CO_2 desorbing during the TPD increased, despite the dramatic decrease in $\theta_{O,res}$. This suggests that the CO coverage at 300 K was greater than 0.25 ML when $\theta_{O,total}$ = 3.74 ML. This would have been possible if the surface area of the metal increased because of surface reconstruction during the CO exposure, or CO formed a higher coverage surface structure. It appears that $\theta_{O,res}$ and the CO_2 yield are indications of two separate processes. Low-temperature CO oxidation, which depletes O_{sub}, occurred *during* the exposure and accounted for the decrease in $\theta_{O,res}$. Therefore, any CO_2 yield in the post-exposure TPD results from reaction between CO (*ad*) and oxygen on the surface. The $\theta_{O,res}$ was whatever was left behind after CO oxidation both during CO exposure and of adsorbed CO during the TPD

experiment. This was supported by the finding that CO_2 yield was unchanged for 30 L and 60 L CO exposures (Table S1) although $\theta_{O,res}$ decreased by 0.18 ML. Although we were unable to quantify the amount of CO_2 formed during exposure, we were able to at least qualitatively estimate the CO coverages from post-exposure STM images and support the notion that most of the oxygen was reacted during exposure. The activation energy for desorption (E_{des}) of CO on Rh(111) is between 134 and 167 kJ mol^{-1}, and CO desorbs at roughly 330 K.[35] Alternatively, CO_2 was only seen to physisorb on Rh(111) as the surface temperature approached 80 K, above which it promptly desorbed.[36] Because CO binds more strongly to the Rh surface than CO_2, it was reasonable that CO molecules remained adsorbed at 300 K while any CO_2 formed during the CO exposures rapidly desorbed and was not detected in TPD experiments.

Because structure determines reactivity, tracking the structural evolution of the O+CO covered Rh(111) surface via STM, as pioneered by Wintterlin and Ertl,[37-39] elucidates the surface sites and species reactive in lower temperature CO oxidation as we observed. Following AO exposure, resulting in $\theta_{O,total}$ = 3.74 ML, the surface displayed the hexagonal RhO_2 moiré along the step edges and (2×1)-O domains on the terraces, displayed as parallel lines along the surface (Figure 2A). Previous work by Gustafson *et al*.[32] suggested that RhO_2 forms along step edges due to oxygen penetration of the crystal at defect sites. As the oxygen concentration increased, growth of the RhO_2 single-layer oxide was observed. It appears that the oxide grew out from the edge on the upper terrace, and although the oxide domains increase with AO exposure, we did not observe completed RhO_2 domains. Additionally, significant O_{sub} forms along with the oxide, and the remaining terraces are covered with the metallic (2×1)-O adlayer; an STM image of the oxidized surface is shown in Figure 2A. The remaining panels in Figure 2 are STM images obtained after increasing CO exposures where $T_{s,CO}$ = 300 K. Figure 2B and 2C are STM images

taken after a 1.5 L CO exposure, where the TPD data in Figure 1 indicated that $\theta_{O,res}$ = 2.49 ML. Both STM images show that CO incorporated into the (2×1)-O adlayer, forming small, isolated (2×2)-O+CO patches. In addition, some disruptions along the boundary between the RhO_2 oxide and the (2×1)-O adlayer were observed. The contrast between the (2×1)-O adlayer and the RhO_2 is clear. Where CO seems to be randomly dispersed throughout the striped (2×1)-O domains, highlighted by the bright pink circles in Figure 2B, the oxide seems to be unaffected, aside from some bright features around what appears to be a defect in the oxide. CO only weakly adsorbs on Rh oxide surfaces, and thus little sticks,[12, 17] therefore CO exposure only disrupted the RhO_2 moiré at defect sites, as indicated by the large cluster of adsorbates in Figure 2B. Further imaging of the sample following CO exposure showed triangular features on the moiré pattern but not on the bare RhO_2 surface (Figure S2). These

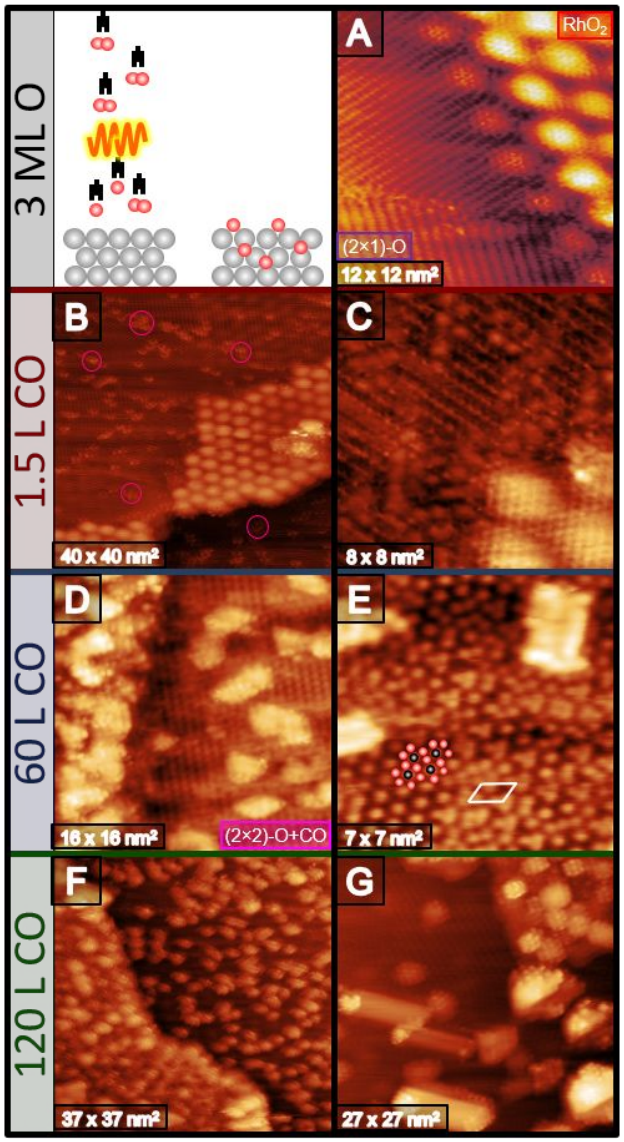

Figure 2. STM images after $T_{s,AO}$ = 700 K and $T_{s,CO}$ = 300 K for various CO exposures. A) RhO_2 243 mV, 301 pA; B) 1.5 L CO, 170 mV, 370 pA; C) 1.5 L CO, 414 mV, 260 pA; D) 60 L CO, -180 mV, -1.38 nA; E) Cartoon of (2×2)-O+CO adlayer and unit cell of dense CO adlayer on Rh(111), 1.04 V, 490 pA; F) 120 L CO, -280 mV, -0.96 nA; G) 400 mV, 175 pA.

triangular structures protrude from the surface, and their lateral spacing remains consistent with the spacing for RhO_2.[32] Protrusions seen along the step edges and defect sites of the moiré suggest that either CO adsorbed or, perhaps reacted away some oxygen, preferentially at these undercoordinated positions.[16] While previous work has suggested that oxygen is replenished by oxygen from RhO_2 during the course of CO oxidation,[12] we saw that the surface composition was essentially unchanged (aside from some CO insertion) after the 1.5 L CO exposure in Figure 2B and 2C in which approximately 1 ML of oxygen was consumed. There must be another source of oxygen: O_{sub}. The terraces remained covered in coexisting domains of the (2×1)-O adlayer and the surface oxide and in any case the surface oxide alone could not account for the approximately 1 ML of O that was removed during the CO exposure. If that were so, the areas of the oxide brims on the terraces would have been significantly reduced; this was not the case. Emergent O_{sub} replenished any surface O reacted during the CO exposure; this supply of O retained the two surface phases. Because it was unlikely that O_{sub} could have regenerated the oxide at 300 K, and the lack of changes to the (2×1)-O domains, the reaction likely took place at the boundary between the two phases. O_{sub} spilling onto the surface maintained the oxygen surface coverage and accounted for the disruptions observed along the boundary.

Figures 2D and 2E show STM images taken after exposing the 3.74 ML O Rh(111) surface to 60 L CO exposure at $T_{s,CO}$ = 300 K. The increased CO exposure, where $\theta_{O,res}$ = 0.07 ML, resulted in much more pronounced changes to the surface than seen after the 1.5 L CO exposure. Little remained of the RhO_2 moiré domain near the step edges, and those areas were now completely consumed by disordered clusters. Additionally, instead of isolated small patches on the terraces, the (2×1)-O adlayer was largely supplanted by the (2×2)-O+CO adlayer. Islands of raised clusters, likely CO stuck on metallic Rh, were also scattered about the terrace. Line

profiles of the internal structure of the disordered clusters on the remnants of RhO_2 domains (Figure S3) were consistent with CO bound directly to Rh in a (√3×√3)R30° overlayer.[40] Intermixed with the (2×2)-O+CO adlayer, trimers formed four membered unit cells (Figure 2E). These features agree with previous work showing dense CO adlayers on Rh(111).[41] As the surface was covered in the (2×1)-O and RhO_2 oxygen domains before CO exposure, the oxygen-depleted domains of (√3×√3)-CO and dense CO structures (Figure 2D and 2E) indicated that nearly *all* oxygen was removed during CO exposure. Because the amount of residual oxygen is so low (0.07 ML O_{res}), it was likely that all the O_{sub} had been depleted, and any further changes to the surface were simply more CO sticking.

The STM images in Figure 2F and 2G show the 3.74 ML O Rh(111) surface after a 120 L CO exposure. This CO exposure gave $\theta_{O,res} < 0.07$ ML, and the STM images show that the surface was completely covered in bright clusters and the (2×2)-O+CO adlayer (Figure 2F) with no evidence of surface oxide or (2×1)-O. The clusters were dispersed throughout the terraces regardless of distance from a step or defect, and the periodicity of the spacing in the bright clusters was (√3×√3)R30° with respect to Rh(111), consistent with CO bound directly to metallic Rh. This surface was entirely denuded of oxygen, aside from the O atoms locked up in the (2×2)-O+CO domains. Because of the excess of CO (on the bare metal patches), nearly all O will oxidize CO in the TPD experiment, leaving behind a vanishingly small amount of residual oxygen, as indicated by the TPD traces in Figure 1. Extensive reconstruction of the surface, such as seen following CO exposure, was consistent with reconstruction seen following extensive oxidation cycles on Rh nanoparticles.[42] In the present study, the presence of O_{sub} and the boundary between RhO_2 and (2×1)-O domains provided low-barrier pathways for CO oxidation

which consumed all oxygen not bound in the stable (2×2)-O+CO adlayer, and left the surface with bare metallic patches and metallic islands, likely remnants of the oxide domains.

In Figure 2, aside from the STM image of the initially prepared oxidized Rh(111) surface (Figure 2A), CO was adsorbed to the surface, as well as whatever oxygen that would go onto react with CO (*ad*) during the TPD ramp. It would be helpful to remove CO (*ad*) to determine how the surface would be changed by CO oxidation during the TPD ramp; furthermore, once CO (*ad*) was removed, any oxygen remaining on the surface would be the residual oxygen quantified in Figure 1. Figure 3 shows a set of STM images of $\theta_{O,total}$ = 3.74 ML Rh(111) surfaces after 10 L and 120 L CO exposures, and annealing at 425 K to remove all CO (*ad*). Because the onset of CO (*ad*) oxidation was ≈ 400 K (Figure S1),[33, 35] annealing at 425 K drove the reaction to completion, leaving behind the residual oxygen, which then allowed determination of the structural consequences of CO exposure and oxidation on the oxidized Rh surface. As shown in Figure 3A, following a 10 L CO exposure at $T_{s,CO}$ = 300 K, the terraces were covered in the (2×2)-O+CO adlayer, and the moiré showed some disturbances at defects and along the step edges. Following the 425 K anneal, the (2×2)-O+CO adlayer was no longer present on the terrace (Figure 3B) because CO (*ad*) was oxidized and desorbed during the TPD ramp, leaving behind the residual O_{ad}. The ordered (2×2)-O+CO domains were replaced by some brighter patches amid regions of what appeared to be (2×2)-O domains in Figure 3B. However, the oxide areas behaved differently. The moiré had several depressions following the 425 K anneal (Figure 3B), but the surface oxide was clearly not perturbed to the extent of the (2×1)-O adlayer. These STM images show that the RhO_2 oxide was unreactive during both the CO exposure and subsequent oxidation of CO (*ad*) with modest CO exposures. Also, the terraces where the metallic (2×1)-O was changed to (2×2)-O+CO by the CO exposure behaved as if there were no

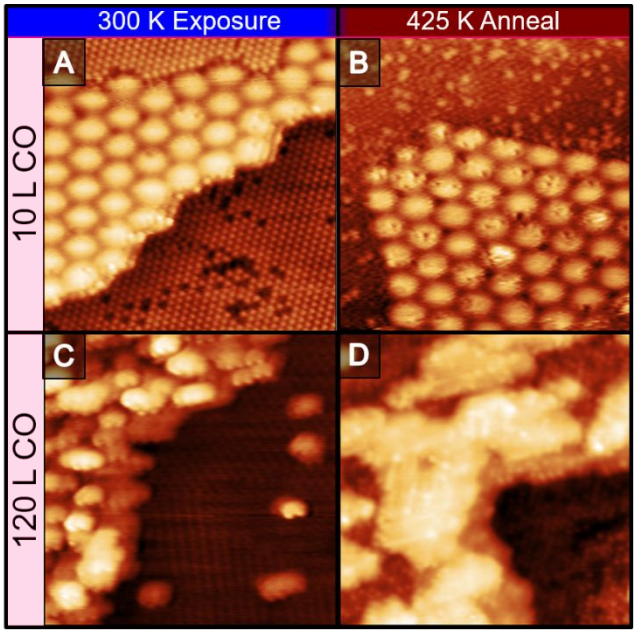

Figure 3. STM images (20 x 20 nm^2) of CO+O/Rh(111) after exposure at $T_{s,CO}$ = 300 K and post-anneal at 425 K, A) 0.65 V, 430 pA; B) -170 mV, -0.74 nA; C) 0.54 V, 300 pA; D) 0.82 V, 305 pA.

O_{sub} or oxide present; the STM images show a similar surface as would result if the entire surface were only (2×2)-O+CO. Although $\theta_{O,res}$ dropped to 1.2 ML, indicating about 2.5 ML O were reacted away *during* the CO exposure, the oxide persisted and the metallic domains were unaltered at T_s = 300 K following CO exposure. Clearly, the reduction in $\theta_{O,res}$ did not come from the surface species, instead its decrease represents the depletion of O_{sub}. Again, because the oxide and metallic domains were unchanged, the reaction must have taken place along the boundary between the two phases, where O_{sub} could access the surface, with some contributions from defects on the oxide, because only those locations are perturbed by the CO exposure.

Although the oxide is essentially unchanged, the disruptions to the moiré suggest that some CO oxidation was occurring at defects on the oxide. Presently, we are unable to distinguish the relative CO oxidation contributions from boundary and oxide defect sites, but some insight arises by combining the observations from the STM images with what is known about oxide surface chemistry. As shown in work by Lewandowski *et al.*,[43] depressions in oxide films following oxidation reactions are indicative of fully reduced regions, and agree with Mars and van Krevelen (MvK) reaction mechanism for catalytic oxidation.[44] Additionally, the

depressions found on the surface oxide following CO exposure and annealing supports that CO_2 was produced during the CO exposure and, through a MvK reaction mechanism, CO was abstracting the oxygen from either surface or lattice bound oxygen, depleting the surface of oxygen and generating depressions in the oxide film, consistent with work done by Zhou *et al*.[45-46] While the observed surface evolution is in agreement with MvK reaction mechanism on the oxide, oxidation along the oxide/(2×1)-O boundary appears to be dominant until O_{sub} is depleted as indicated by the conservation of the surface oxide at 10 L CO exposure and the disruptions along the (2×1)-O/moiré domain boundaries at modest CO exposures.

When the CO exposure was increased to 120 L at $T_{s,CO}$ = 300 K, as shown in Figure 3C, the STM image showed extensive CO adsorption, and as discussed previously, little oxygen remained on the surface. The terraces were significantly covered by domains of the (2×2)-O+CO with dispersed bright islands. The top of the step edges, where the oxide was before CO exposure, was entirely disrupted by raised clusters of dense CO/Rh adlayers. When this surface was annealed to 425 K (Figure 3D), the bright clusters along the step edge evolved to several large islands where linear patterns were evident. The terrace was also covered in patches of hexagonally arranged adsorbates and smaller depressed, dark regions. If CO only reacted at higher temperatures after adsorption, then the surface evolution would be invariant for all CO exposures; the surface would be saturated with CO in either case. The difference between the 10 L and 120 L CO exposure surfaces following a 425 K anneal suggests that the surface was changing during the course of the CO exposure, therefore more CO consumed O. Additionally, the (2×1)-O adlayer and oxygen at domain boundaries was reacted by smaller CO exposures and the surface oxide was consumed after longer CO exposures. Our results are in agreement with Gustafson *et al*.,[17] who showed the (2×1)-O phase to be more active than the surface oxide

during CO oxidation. However, as reported previously,[12] although the metallic terraces were more reactive, O atoms migrating from the oxide at elevated temperatures provided a steady supply of O for CO oxidation. However, our CO exposures were performed at 300 K, where surface bound O was less mobile than the previous work done at 375 K.[12] Furthermore, the persistence of the oxide suggests that, although it is eventually consumed, the lag in its destruction was because there was another source of oxygen: O_{sub}. Once O_{sub} was depleted, then the oxide was attacked by CO. Again, we are presently unable to determine the relative rates of oxidation on oxide defects and along the boundary, this is an issue we will be pursuing in the future.

Finally, the extent of CO oxidation at decreased $T_{S,CO}$ was considered. In order to determine the lower temperature limit of CO oxidation, we repeated CO exposure to the oxidized surface at $T_{s,CO}$ = 200 K and compared the results to identical CO exposures done at $T_{s,CO}$ = 300 K (Figure 4). For each 10L exposure (Figure 4A and 4C), the terraces were covered in the (2×2)-O+CO adlayer, and Figure 4A shows an island of what was surface oxide moiré completely covered in the (2×2)-O+CO adlayer. In addition, this island of surface oxide also had some bright clusters forming, similar to those seen in Figure 2 and 3, suggesting surface evolution at temperatures well below the CO oxidation reaction

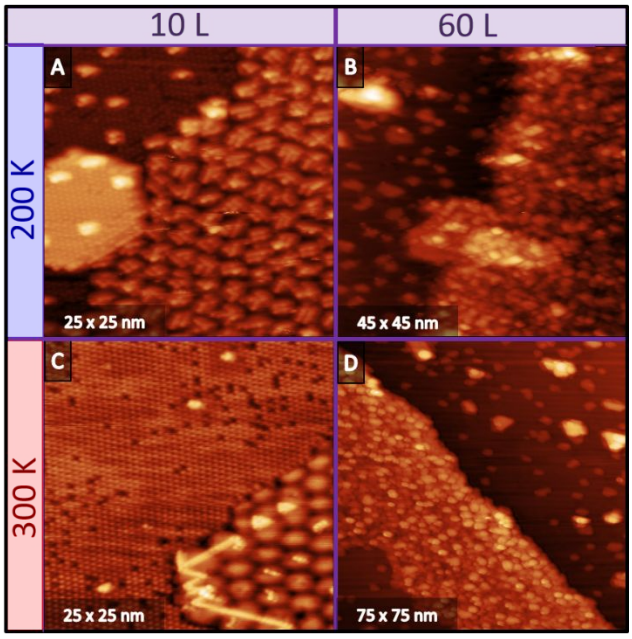

Figure 4. STM images of oxidized Rh(111) following CO exposure at $T_{s,CO}$ = 300 K and 200 K. A) -1.22 V, -0.92 nA; B) -0.85 V, -0.70 nA; C) 450 mV, 400 pA; D) 0.54 V, 300 pA.

temperature. Figure 4A shows regular, linear decoration interrupting the hexagonal moiré pattern at 200 K. Alternatively, the surface oxide in Figure 4C shows very few adsorbates. Rather, there are sparse, bright adsorbates along the surface oxide/(2×1)-O boundary, and on some oxide defects. The relative number of defects at 200 and 300 K suggests that the lower surface temperature allowed for CO to adsorb to the surface oxide without the presence of extensive defects. Therefore, at lower temperatures, CO adsorption to the surface oxide was favorable, despite the reduced interaction with CO at elevated temperatures. For the 60L CO exposure (Figure 4B and 4D), clusters replaced the surface oxide, and islands began to form on the terrace as seen previously (Figure 2 and 3). The similar structural evolution of the surface following CO exposure at $T_{s,CO}$ = 200 K and 300 K indicates low temperature CO oxidation was occurring, but as was seen in Figure 3, there was no discrimination between surface sites at higher CO exposures.

Conclusion

In this study, we demonstrated O_{sub} provides the means for low temperature CO oxidation on highly oxidized Rh(111) surfaces with a mixture of (2×1)-O and RhO_2 domains. STM images showed little changes to the surface after modest CO exposures where a dramatic decrease in the amount of oxygen was observed. CO was seen to adsorb along the (2×1)-O and RhO_2 domains, and along (2×1)-O domain boundaries. This suggests that the reaction occurred along the interfaces of the co-existing domains at 300 K and below, and O_{sub} replenished the reacted oxygen. Prolonged CO exposures consumed all O_{sub} and reacted away the oxide starting at defect sites. Additionally, we have demonstrated that at 200 K, CO was bound to the surface oxide at modest exposures, and the surface undergoes reconstruction during the exposure at 200 K. This suggests that, while the metallic O_{ad} phase may be important at elevated temperatures

for CO oxidation, control of the sample temperature can activate CO oxidation on the surface oxide. The importance of increased oxygen concentration for lowering the activation energy for oxidation has been demonstrated and confirms the key roles of surface oxide and subsurface oxygen in catalytic oxidation, in addition to the metallic O_{ad} phase.

ASSOCIATED CONTENT

Supporting Information. Supporting information is provided as a separate document and contains supporting TPD data, image line profiles, and STM images (.doc). This information is available free of charge on the ACS Publications website.

Corresponding Author

*Tel.: (773) 508-3136. E-mail: dkillelea@luc.edu.

Author Contributions

The manuscript was written through contributions of all authors. All authors have given approval to the final version of the manuscript.

Acknowledgement

Acknowledgement is made to the Donors of the American Chemical Society Petroleum Research Fund for partial support of this research through Grant PRF #54770-DNI5. We also wish to acknowledge partial support from the National Science Foundation (CHE-1800291). This work was also supported by the College of Arts and Sciences at Loyola University Chicago. R. G. Farber thanks The Arthur J. Schmitt Foundation for support during this work. We also wish to thank Dr. Kevin Gibson for valuable discussions.

References

(1) Devarajan, S. P.; Hinojosa Jr., J. A.; Weaver, J. F. STM Study of High-Coverage Structures of Atomic Oxygen on Pt(111): p(2×1) and Pt Oxide Chain Structures. *Surf. Sci.* **2008,** *602*, 3116-3124.
(2) Weaver, J. F. Surface Chemistry of Late Transition Metal Oxides. *Chem. Rev.* **2013,** *113*, 4164-4215.
(3) Farber, R. G.; Turano, M. E.; Oskorep, E. C. N.; Wands, N. T.; Iski, E. V.; Killelea, D. R. The Quest for Stability: Structural Dependence of Rh(111) on Oxygen Coverage at Elevated Temperature. *J. Phys. Chem. C* **2017,** *121*, 10470 – 10475.
(4) Derouin, J.; Farber, R. G.; Turano, M. E.; Iski, E. V.; Killelea, D. R. Thermally Selective Formation of Subsurface Oxygen in Ag(111) and Consequent Surface Structure. *ACS Catal.* **2016,** *6*, 4640-4646.
(5) Derouin, J.; Farber, R. G.; Killelea, D. R. Combined STM and TPD Study of Rh(111) Under Conditions of High Oxygen Coverage. *J. Phys. Chem. C* **2015,** *119*, 14748-14755.
(6) Gustafson, J.; Westerström, R.; Mikkelsen, A.; Torrelles, X.; Balmes, O.; Bovet, N.; Andersen, J. N.; Baddeley, C. J.; Lundgren, E. Sensitivity of Catalysis to Surface Structure: The Example of CO Oxidation on Rh Under Realistic Conditions *Phys. Rev. B* **2008,** *78*, 045423.
(7) Montano, M.; Tang, D. C.; Somorjai, G. A. Scanning Tunneling Microscopy (STM) at High Pressures. Adsorption and Catalytic Reaction Studies on Platinum and Rhodium Single Crystal Surfaces. *Catal. Lett.* **2006,** *107*, 131-141.
(8) Herbschleb, C. T.; van der Tuijn, P. C.; Roobol, S. B.; Navarro, V.; Bakker, J. W.; Liu, Q.; Stoltz, D.; Canas-Ventura, M. E.; Verdoes, G.; van Spronsen, M. A.; Bergman, M.; Crama, L.; Taminiau, I.; Ofitserov, A.; van Baarle, G. J. C.; Frenken, J. W. M. The ReactorSTM: Atomically Resolved Scanning Tunneling Microscopy Under High-Pressure, High-Temperature Catalytic Reaction Conditions. *Rev. Sci. Instrum.* **2014,** *85*, 083703.
(9) Salmeron, M.; Schlogl, R. Ambient Pressure Photoelectron Spectroscopy: A New Tool for Surface Science and Nanotechnology. *Surf. Sci. Rep.* **2008,** *63*, 169-199.
(10) Goodman, D. W. Correlations Between Surface Science Models and "Real-World" Catalysts. *J. Phys. Chem.* **1996,** *100*, 13090-13102.
(11) Reuter, K.; Scheffler, M. Composition, Structure, and Stability of RuO_2(110) as a Function of Oxygen Pressure. *Phys. Rev. B* **2001,** *65*, 035406.
(12) Lundgren, E.; Gustafson, J.; Resta, A.; Weissenrieder, J.; Mikkelsen, A.; Andersen, J. N.; Kohler, L.; Kresse, G.; Klikovits, J.; Biederman, A.; Schmid, M.; Varga, P. The Surface Oxide as a Source of Oxygen on Rh(111). *J. Electron. Sprectrosc. Relat. Phenom.* **2005,** *144*, 367-372.
(13) Freund, H. J. The Surface Science of Catalysis and More, Using Ultrathin Oxide Films as Templates: A Perspective. *J. Am. Chem. Soc.* **2016,** *138*, 8985-8996.
(14) Kim, S. M.; Qadir, K.; Seo, B.; Jeong, H. Y.; Joo, S. H.; Terasaki, O.; Park, J. Y. Nature of Rh Oxide on Rh Nanoparticles and Its Effect on the Catalytic Activity of CO Oxidation. *Catal. Lett.* **2013,** *143*, 1153-1161.
(15) Gao, F.; McClure, S.; Chen, M.; Goodman, D. W. Comment on "Catalytic Activity of the Rh Surface Oxide: CO Oxidation over Rh(111) under Realistic Conditions". *J. Phys. Chem. C* **2010,** *114*, 22369-22371.
(16) Gustafson, J.; Westerstrom, R.; Balmes, O.; Resta, A.; van Rijn, R.; Torrelles, X.; Herbschleb, C. T.; Frenken, J. W. M.; Lundgren, E. Catalytic Activity of the Rh Surface Oxide: CO Oxidation over Rh(111) under Realistic Conditions. *J. Phys. Chem. C* **2010,** *114*, 4580-4583.

(17) Gustafson, J.; Balmes, O.; Zhang, C.; Shipilin, M.; Schaefer, A.; Hagman, B.; Merte, L. R.; Martin, N. M.; Carlsson, P. A.; Jankowski, M.; Crumlin, E. J.; Lundgren, E. The Role of Oxides in Catalytic CO Oxidation over Rhodium and Palladium. *ACS Catal.* **2018,** *8*, 4438-4445.
(18) Gustafson, J.; Westerström, R.; Balmes, O.; Resta, A.; van Rijn, R.; Torrelles, X.; Herbschleb, C. T.; Frenken, J. W. M.; Lundgren, E. Reply to "Comment on 'Catalytic Activity of the Rh Surface Oxide: CO Oxidation over Rh(111) under Realistic Conditions"'. *J. Phys. Chem. C* **2010,** *114*, 22372-22373.
(19) McClure, S. M.; Lundwall, M.; Yang, F.; Zhou, Z.; Goodman, D. W. CO Oxidation on $Rh/SiO_2/Mo(112)$ Model Catalysts at Elevated Pressures. *J. Phys. Chem. C* **2009,** *113*, 9688-9697.
(20) Bian, Y.; Kim, M.; Li, T.; Asthagiri, A.; Weaver, J. F. Facile Dehydrogenation of Ethane on the $IrO_2(110)$ Surface. *J. Am. Chem. Soc.* **2018,** *140*, 2665-2672.
(21) Liang, Z.; Li, T.; Kim, M.; Asthagiri, A.; Weaver, J. F. Low-Temperature Activation of Methane on the $IrO_2(110)$ Surface. *Science* **2017,** *356*, 299-303.
(22) Derouin, J.; Farber, R. G.; Heslop, S. L.; Killelea, D. R. Formation of Surface Oxides and Ag_2O Thin Films with Atomic Oxygen on Ag(111). *Surf. Sci.* **2015,** *641*, L1-4.
(23) Umemoto, H.; Kusanagi, H. Catalytic Decomposition of O_2, NO, N_2O, and NO_2 on a Heated Ir Filament to Produce Atomic Oxygen. *J. Phys. D: Appl. Phys.* **2008,** *41*, 225505.
(24) Kolb, M. J.; Farber, R. G.; Derouin, J.; Badan, C.; Calle-Vallejo, F.; Juurlink, L. B. F.; Killelea, D. R.; Koper, M. T. M. Double-Stranded Water on Stepped Platinum Surfaces. *Phys. Rev. Lett.* **2016,** *116*, 136101.
(25) Matsushima, T.; Matsui, T.; Hashimoto, M. Kinetic Studies on the CO Oxidation on a Rh(111) Surface by Means of Angle-Resolved Thermal Desorption. *J. Chem. Phys.* **1984,** *81*, 5151.
(26) Jaworowski, A. J.; Beutler, A.; Strisland, F.; Nyholm, R.; Setlik, B.; Heskett, D.; Andersen, J. N. Adsorption Sites in O And CO Coadsorption Phases on Rh(111) Investigated by High-Resolution Core-Level Photoemission. *Surf. Sci.* **1999,** *431*, 33-41.
(27) Hopstaken, M. J. P.; Niemantsverdriet, J. W. Structure Sensitivity in the CO Oxidation on Rhodium: Effect of Adsorbate Coverages on Oxidation Kinetics on Rh(100) and Rh(111). *J. Chem. Phys.* **2000,** *113*, 5457-5465.
(28) Krenn, G.; Bako, I.; Schennach, R. CO Adsorption and CO and O Coadsorption on Rh(111) Studied by Reflection Absorption Infrared Spectroscopy and Density Functional Theory. *J. Chem. Phys.* **2006,** *124*, 144703.
(29) Marchini, S.; Sachs, C.; Wintterlin, J. STM Investigation of the (2×2)O and (2×1)O Structures on Rh(111). *Surf. Sci.* **2005,** *592*, 58-64.
(30) Kizilkaya, A. C.; Gracia, J. M.; Niemantsverdriet, J. W. A Direct Relation between Adsorbate Interactions, Configurations, and Reactivity: CO Oxidation on Rh(100) and Rh(111). *J. Phys. Chem. C* **2010,** *114*, 21672-21680.
(31) Schwegmann, S.; Over, H.; DeRenzi, V.; Ertl, G. The Atomic Geometry of the O and CO+O Phases on Rh(111). *Surf. Sci.* **1997,** *375*, 91-106.
(32) Gustafson, J.; Mikkelsen, A.; Borg, M.; Lundgren, E.; Kohler, L.; Kresse, G.; Schmid, M.; Varga, P.; Yuhara, J.; Torrelles, X.; Quiros, C.; Andersen, J. N. Self-Limited Growth of a Thin Oxide Layer on Rh(111). *Phys. Rev. Lett.* **2004,** *92*, 126102.
(33) Gibson, K. D.; Killelea, D. R.; Sibener, S. J. Comparison of the Surface and Subsurface Oxygen Reactivity and Dynamics with CO Adsorbed on Rh(111). *J. Phys. Chem. C* **2014,** *118*, 14977-14982.

(34) Gibson, K. D.; Viste, M.; Sanchez, E. C.; Sibener, S. J. High Density Adsorbed Oxygen on Rh(111) and Enhanced Routes to Metallic Oxidation Using Atomic Oxygen. *J. Chem. Phys.* **1999,** *110*, 2757-2760.
(35) Campbell, C. T.; White, J. M. The Adsorption, Desorption, and Reactions of CO and O_2 on Rh. *J. Catal.* **1978,** *54*, 289-302.
(36) Freund, H. J.; Roberts, M. W. Surface Chemistry of Carbon Dioxide. *Surf. Sci. Rep.* **1996,** *25*, 225-273.
(37) Rößler, M.; Geng, P.; Wintterlin, J. A High-Pressure Scanning Tunneling Microscope for Studying Heterogeneous Catalysis. *Rev. Sci. Instrum.* **2005,** *76*, 023705.
(38) Wintterlin, J. "Scanning Tunneling Microscopy Studies of Catalytic Reactions" In *Advances in Catalysis*, Academic Press: Cambridge, MA USA, 2000; Vol. 45, pp 131-206.
(39) Zambelli, T.; Wintterlin, J.; Trost, J.; Ertl, G. Identification of the "Active Sites" of a Surface-Catalyzed Reaction. *Science* **1996,** *273*, 1688-1690.
(40) Thiel, P. A.; Williams, E. D.; Yates, J. T.; Weinberg, W. H. The Chemisorption of CO on Rh(111). *Surf. Sci.* **1979,** *84*, 54-64.
(41) Cernota, P.; Rider, K.; Yoon, H. A.; Salmeron, M.; Somorjai, G. Dense Structures Formed by CO on Rh(111) Studied by Scanning Tunneling Microscopy. *Surf. Sci.* **2000,** *445*, 249-255.
(42) Nolte, P.; Stierle, A.; Jin-Phillipp, N. Y.; Kasper, N.; Schulli, T. U.; Dosch, H. Shape Changes of Supported Rh Nanoparticles During Oxidation and Reduction Cycles. *Science* **2008,** *321*, 1654-1658.
(43) Lewandowski, M.; Groot, I. M. N.; Shaikhutdinov, S.; Freund, H. J. Scanning Tunneling Microscopy Evidence for the Mars-Van Krevelen Type Mechanism of Low Temperature CO Oxidation on an FeO(111) Film on Pt(111). *Catal. Today* **2012,** *181*, 52-55.
(44) Doornkamp, C.; Ponec, V. The Universal Character of the Mars and van Krevelen Mechanism. *J. Mol. Catal. A: Chem.* **2000,** *162*, 19-32.
(45) Zhou, X.; Shen, Q.; Yuan, K.; Yang, W.; Chen, Q.; Geng, Z.; Zhang, J.; Shao, X.; Chen, W.; Xu, G.; Yang, X.; Wu, K. Unraveling Charge State of Supported Au Single-Atoms during CO Oxidation. *J. Am. Chem. Soc.* **2018,** *140*, 554-557.
(46) Zhou, X.; Yang, W.; Chen, Q.; Geng, Z.; Shao, X.; Li, J.; Wang, Y.; Dai, D.; Chen, W.; Xu, G.; Yang, X.; Wu, K. Stable Pt Single Atoms and Nanoclusters on Ultrathin CuO Film and Their Performances in CO Oxidation. *J. Phys. Chem. C* **2016,** *120*, 1709-1715.

Table of Contents Graphic

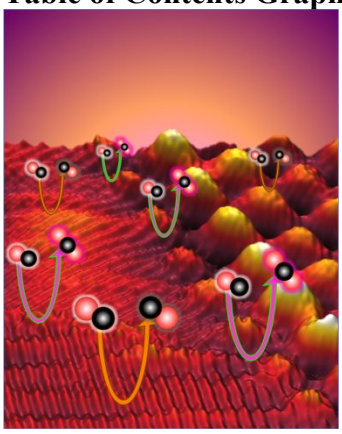

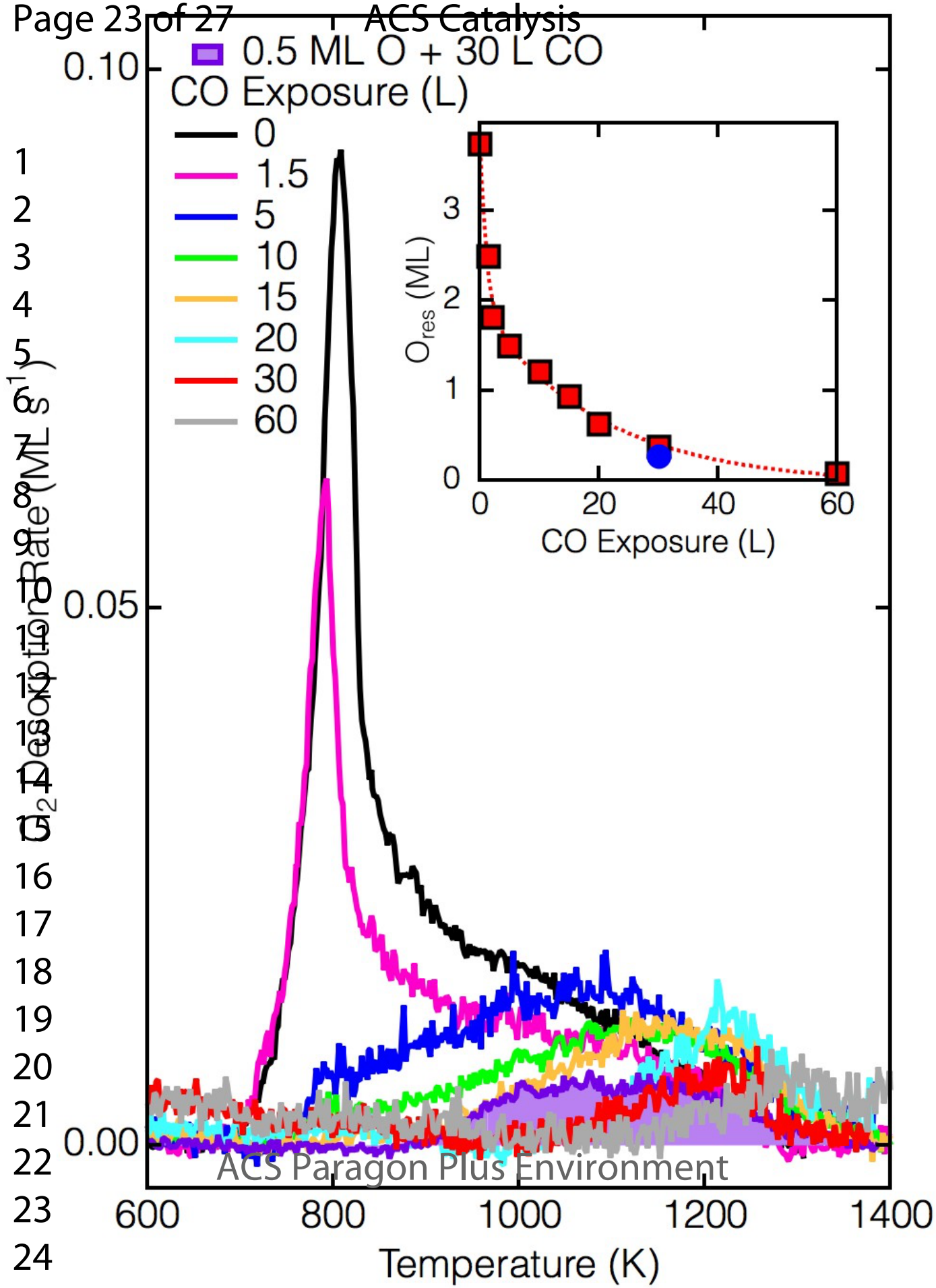
0.5 ML O + 30 L CO
CO Exposure (L)
0
1.5
5
10
15
20
30
60
0.10
0.05
0.00
O_2 Desorption Rate (ML s^{-1})
O_{res} (ML)
CO Exposure (L)
600
800
1000
1200
1400
Temperature (K)
ACS Paragon Plus Environment

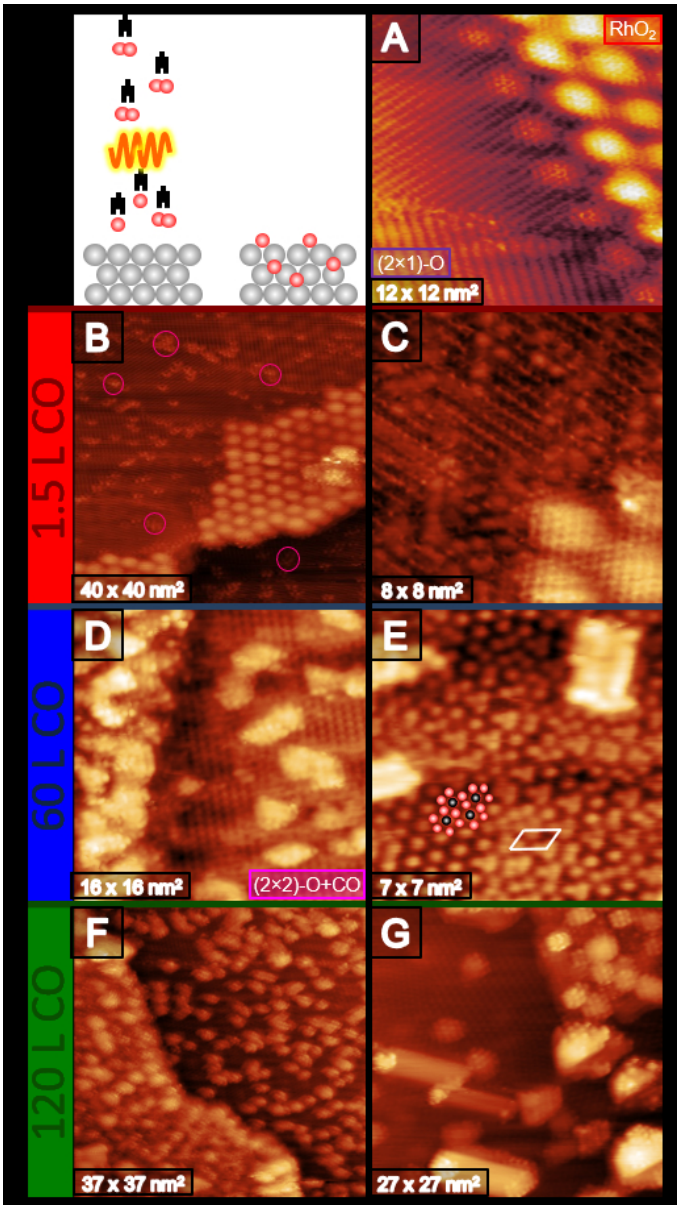

Figure 2. STM images after Ts,AO = 700 K and Ts,CO = 300 K for various CO exposures. A) RhO2 243 mV, 301 pA; B) 1.5 L CO, 170 mV, 370 pA; C) 1.5 L CO, 414 mV, 260 pA; D) 60 L CO, -180 mV, -1.38 nA; E) Cartoon of (2×2)-O+CO adlayer and unit cell of dense CO adlayer on Rh(111), 1.04 V, 490 pA; F) 120 L CO, -280 mV, -0.96 nA; G) 400 mV, 175 pA.

86x154mm (150 x 150 DPI)

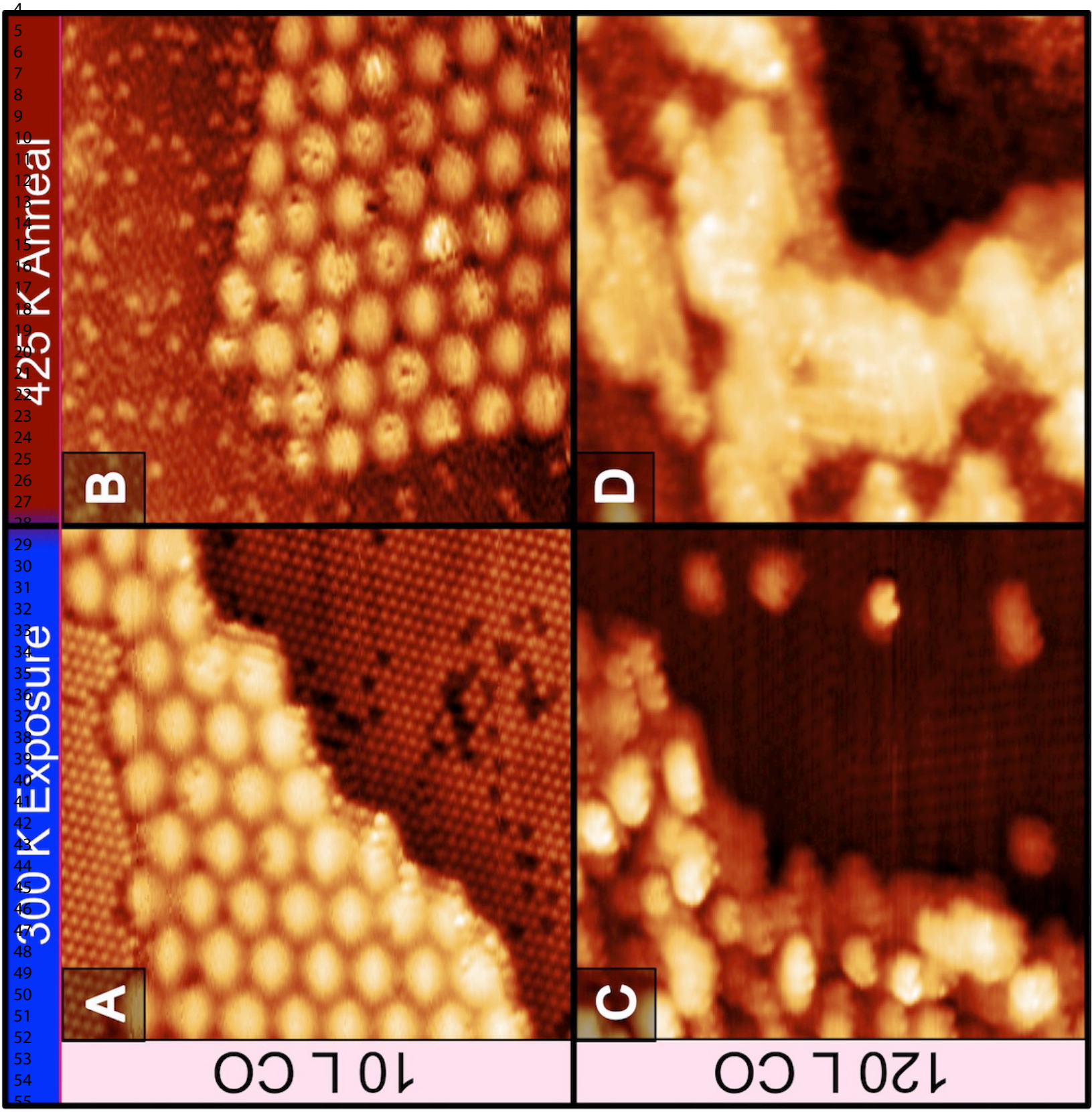
425 K Anneal
300 K Exposure
B
D
A
C
10 L CO
120 L CO

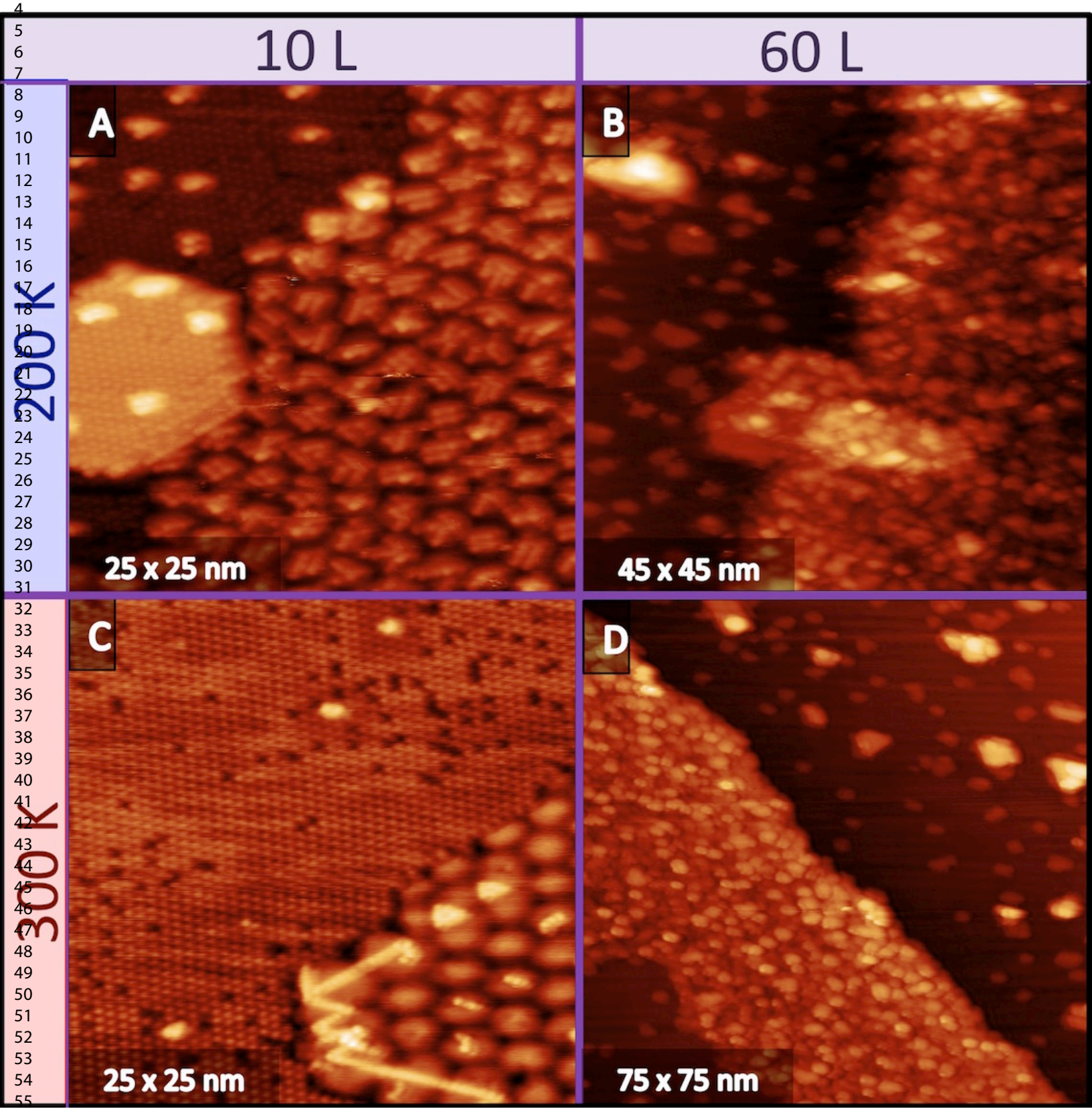
10 L
60 L
200 K
300 K
A
B
C
D
25 x 25 nm
45 x 45 nm
25 x 25 nm
75 x 75 nm

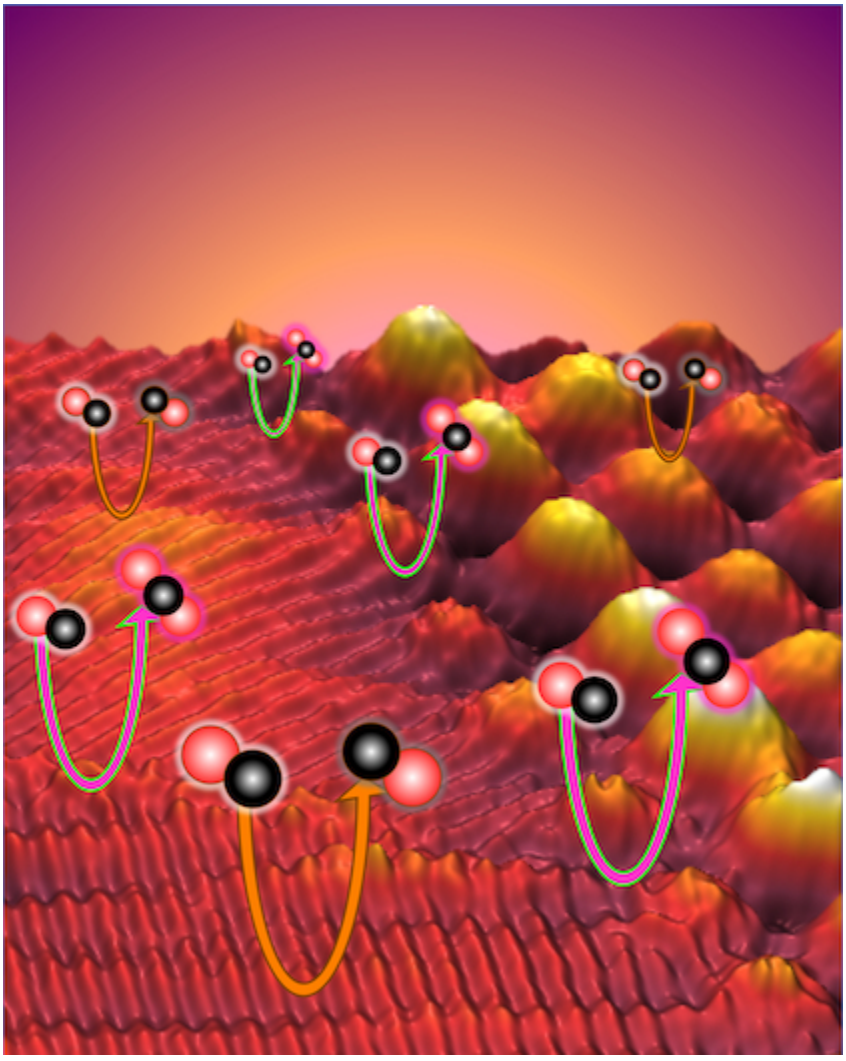

TOC Image

35x44mm (300 x 300 DPI)